Inorg. Chem. **2003**, *42*, 6032–6040

Slow Electron Transfer Rates for Fluorinated Cobalt Porphyrins: Electronic and Conformational Factors Modulating Metalloporphyrin ET

Haoran Sun, Valeriy V. Smirnov, and Stephen G. DiMagno*

Department of Chemistry, University of Nebraska—Lincoln, Lincoln, Nebraska 68588-0304

Received June 20, 2003

The electron transfer (ET) properties of a series of closely related cobalt porphyrins, [2,3,7,8,12,13,17,18-octafluoro-5,10,15,20-tetrakis(pentafluorophenyl)porphyrinato]cobalt, $CoF_{28}TPP$, [2,3,7,8,12,13,17,18-octafluoro-5,10,15,20-tetraphenyl)porphyrinato]cobalt, CoF_8TPP, 5,10,15,20-tetrakis(pentafluorophenyl)porphyrinato]cobalt, $CoF_{20}TPP$, and [5,10,15,20-tetraphenylporphyrinato]cobalt, CoTPP, were investigated by cyclic voltammetry, cyclic voltammetric digital simulation, in situ UV–vis and IR spectroelectrochemistry, kinetic ET studies, bulk electrolysis, ^{19}F NMR spectroscopy, X-ray crystallography, and molecular modeling. In benzonitrile containing 0.1 M tetrabutylammonium hexafluorophosphate ($TBAPF_6$) as supporting electrolyte, the ET rate constants for the $Co^{2+/3+}$ redox couples were found to be strongly substituent dependent; the heterogeneous ET rate constant (k_{el}) varied by a factor of 10^4, and the ET self-exchange rate constants (k_{ex}) varied over 7 orders of magnitude for the compounds studied. The remaining observed ring oxidation and metal and ring reduction events exhibited nearly identical k_{el} values for all compounds. UV–vis and IR spectroelectrochemistry, bulk electrolysis, and ^{19}F NMR spectroscopic studies support attribution of different ET rates to widely varying inner sphere reorganization energies (λ_i) for these closely related compounds. Structural and semiempirical (PM3) studies indicate that the divergent kinetic behavior of CoTPP, CoF_8TPP, $CoF_{20}TPP$, and $CoF_{28}TPP$ first oxidations arises mainly from large nuclear reorganization energies primarily associated with core contraction and dilation. Taken together, these studies provide rational design principles for modulating ET rate constants in cobalt porphyrins over an even larger range and provide strategies for similar manipulation of ET rates in other porphyrin-based systems: substituents that lower C–C, C–N, and N–M vibrational frequencies or minimize porphyrin orbital overlap with the metal-centered orbital undergoing a change in electron population will increase k_{ET}. The heme ruffling apparent in electron transfer proteins such as cytochrome *c* is interpreted as nature's exploitation of this design strategy.

Introduction

Owing to their utility as functional models for naturally occurring hemes,[1−4] cobalt porphyrins have been subjected to a wide range of electrochemical and electron transfer (ET) studies.[5] It has long been noted that the metal-centered oxidation of cobalt ($Co^{2+/3+}$) in porphyrins exhibits sluggish heterogeneous and homogeneous ET rates in comparison to porphyrin ring oxidation, to ring or metal reduction, or to the analogous $Fe^{2+/3+}$ oxidation in iron porphyrins.[5] For example, self-exchange ET rate constants (k_{ex}) for 5,10,15,20-tetraarylmetalloporphyrins fall in the range 10^{-2} to 10^4 M^{-1} s^{-1} for the $Co^{2+/3+}$ process,[6] and 10^7 to 10^8 M^{-1} s^{-1} for the $Fe^{2+/3+}$ process.[7−10] As studies of cobalt cytochrome *c* have demonstrated, the reduction in k_{ex} for the oxidation of Co^{2+} porphyrins is primarily due to large inner sphere reorganization energies ($\lambda_i \sim 2.4$ eV).[11] Because Co^{2+} porphyrins are

(1) Chien, J. C. W.; Gibson, H. L.; Dickinson, L. C. *Biochemistry* **1978**, *17*, 2579−84.
(2) Jones, R. D.; Summerville, D. A.; Basolo, F. *Chem. Rev.* **1979**, *79*, 139−79.
(3) Anson, F. C.; Shi, C.; Steiger, B. *Acc. Chem. Res.* **1997**, *30*, 437−444.
(4) Collman, J. P.; Fu, L.; Herrmann, P. C.; Zhang, X. *Science (Washington, D.C.)* **1997**, *275*, 949−951.
(5) Fukuzumi, S. In *The Porphyrin Handbook*; Guilard, R., Ed.; Academic Press: San Diego, CA, 2000; Vol. 8, pp 115−151.
(6) Chapman, R. D.; Fleischer, E. B. *J. Am. Chem. Soc.* **1982**, *104*, 1575−82.
(7) Dixon, D. W.; Woehler, S.; Hong, X.; Stolzenberg, A. M. *Inorg. Chem.* **1988**, *27*, 3682−5.
(8) Shirazi, A.; Barbush, M.; Ghosh, S.; Dixon, D. W. *Inorg. Chem.* **1985**, *24*, 2495−502.
(9) Dixon, D. W.; Barbush, M.; Shirazi, A. *Inorg. Chem.* **1985**, *24*, 1081−7.
(10) Dixon, D. W.; Barbush, M.; Shirazi, A. *J. Am. Chem. Soc.* **1984**, *106*, 4638−9.

10.1021/ic034705o CCC: $25.00
Published on Web 08/28/2003

generally low spin ($S = {}^1/_2$), removal of an electron from the predominantly d_{z^2}-character HOMO results in large changes in the bonding about the cobalt ion, including significant alteration of the metal−nitrogen bond distances and an associated contraction of the macrocycle framework around the smaller ion.

Due to their more positive redox potentials and higher stability compared to their nonhalogenated counterparts, metalloporphyrins possessing halogen (F, Cl, Br) at the pyrrole (β) positions and/or *meso*-haloaryl or *meso*-haloalkyl substituents have garnered interest as potential catalysts for the oxidation of organic substrates, including alkane hydroxylation and alkene epoxidation.[12−34] Recently, we reported the synthesis and unusual properties of β-octafluorinated porphyrins and their zinc, cobalt, and rhodium derivatives.[35−38] A key advantage offered by fluorine substituents is that their relatively small size allows electronic effects to be studied independently of the profound steric and/or conformational perturbations that are seen with larger halogens. Here, we show that the magnitudes of the ET kinetic rate constants for the metal-centered ($Co^{2+/3+}$) oxidation are unusually small and very sensitive to the degree of fluorine substitution. These results contrast with electrochemical studies of β-brominated Co^{2+} tetraarylporphyrins, which show halogen substitution correlated with an increase in k_{el} for the $Co^{2+/3+}$ couple.[39] The juxtaposition of these studies generates an interesting puzzle: why should apparently similar β-octahalogenated ligand systems give rise to such different ET kinetic behavior for the chelated cobalt ion? The answer to this question provides a general design strategy for manipulating ET rate constants in metalloporphyrins.

Experimental Section

Materials. Materials were obtained from Aldrich Chemical Co., unless otherwise noted. Benzonitrile and deuterated benzene (Cambridge Isotope Laboratories) were distilled under reduced pressure from P_2O_5 and redistilled from CaH_2. Acetonitrile was distilled from P_2O_5 and redistilled from $AgPF_6$. Pyridine and CH_2Cl_2 were distilled from CaH_2. Tetra-*n*-butylammonium hexafluorophosphate ($TBAPF_6$) (Fluka) was thrice recrystallized from acetone/ether and dried under vacuum (18 h, 40 °C) prior to use. Hexafluorobenzene was used as an internal chemical shift reference ($\delta = -164.9$ ppm) for ^{19}F NMR experiments. All other reagents were of analytical grade. CoF_8TPP, $CoF_{28}TPP$, and $CoF_{20}TPP$ were synthesized by literature procedures.[37] CoTPP was recrystallized from toluene before use.

Instrumentation and Methods. Electrochemical experiments were performed with either a computer-controlled EG&G PARC M273 potentiostat with M270 electrochemical software or with an EG&G PARC M173 potentiostat. For cyclic voltammetry, a three-electrode system consisting of a planar platinum working electrode (EG&G, 0.0314 cm^2), a platinum wire counter electrode, and a reference electrode was employed. The reference electrode was either Ag/Ag^+ (0.01 M $AgNO_3$ in CH_3CN with 0.1 M $TBAPF_6$) or a silver wire quasi-reference electrode. The observed potential was corrected by comparison to an internal standard, Fc/Fc^+ ($E_{1/2} = 151 \pm 3$ mV vs Ag/Ag^+). All potentials reported in this paper are referenced to the Ag/Ag^+ couple. The working electrode was polished and cleaned ultrasonically prior to each use. In situ UV−vis and FTIR spectroelectrochemical experiments were performed with an optically transparent, adjustable path length, thin-layer spectroelectrochemical cell.[40] A Pt grid was used as the working electrode; two Pt sheets were used as the counter electrode. UV−vis spectra were recorded on an Olis-14 modification of a Cary-14 spectrophotometer. The bulk electrolysis cell possessed two chambers separated by a fine fritted disk. Two large area Pt grid electrodes were used as working and counter electrodes. A homemade Ag/Ag^+ (0.01 M $AgNO_3$ in CH_3CN including 0.1 M $TBAPF_6$) reference electrode was separated from the bulk of the solution by a Luggin capillary containing $TBAPF_6$ (0.5 M) in benzonitrile. UV−vis spectra after bulk electrolysis were determined in a Schlenk-style cell and compared with the in situ spectroelectrochemical results. Digisim 3.05 software (Bioanalytical Systems Inc.) was used for cyclic voltammetric digital simulation.

Further experimental details concerning the X-ray crystal structure determination, stopped-flow kinetic runs, Marcus cross-

(11) Sun, J.; Su, C.; Wishart, J. F. *Inorg. Chem.* **1996**, *35*, 5893−5901.
(12) Chauhan, S. M. S.; Kandadai, S. A.; Sahoo, B. *Chem. Pharm. Bull.* **2001**, *49*, 1375−1376.
(13) Gonsalves, A. M. d. A. R.; Serra, A. C. *J. Porphyrins Phthalocyanines* **2000**, *4*, 598−603.
(14) Hino, F.; Dolphin, D. *Chem. Commun.* **1999**, 629−630.
(15) Birnbaum, E. R.; Le Lacheur, R. M.; Horton, A. C.; Tumas, W. *J. Mol. Catal. A: Chem.* **1999**, *139*, 11−24.
(16) Groves, J. T.; Shalyaev, K. V.; Bonchio, M.; Carofiglio, T. *Stud. Surf. Sci. Catal.* **1997**, *110*, 865−872.
(17) Boettcher, A.; Birnbaum, E. R.; Day, M. W.; Gray, H. B.; Grinstaff, M. W.; Labinger, J. A. *J. Mol. Catal. A: Chem.* **1997**, *117*, 229−242.
(18) Iwanejko, R.; Battioni, P.; Mansuy, D.; Mlodnicka, T. *J. Mol. Catal. A: Chem.* **1996**, *111*, 7−9.
(19) Battioni, P.; Iwanejko, R.; Mansuy, D.; Mlodnicka, T.; Poltowicz, J.; Sanchez, F. *J. Mol. Catal. A: Chem.* **1996**, *109*, 91−98.
(20) Lyons, J. E.; Ellis, P. E., Jr.; Myers, H. K., Jr. *J. Catal.* **1995**, *155*, 59−73.
(21) Labinger, J. A. *Catal. Lett.* **1994**, *26*, 95−9.
(22) Chen, H. L.; Ellis, P. E., Jr.; Wijesekera, T.; Hagan, T. E.; Groh, S. E.; Lyons, J. E.; Ridge, D. P. *J. Am. Chem. Soc.* **1994**, *116*, 1086−9.
(23) Battioni, P.; Bartoli, J. F.; Mansuy, D.; Byun, Y. S.; Traylor, T. G. *J. Chem. Soc., Chem. Commun.* **1992**, 1051−3.
(24) Traylor, T. G.; Hill, K. W.; Fann, W. P.; Tsuchiya, S.; Dunlap, B. E. *J. Am. Chem. Soc.* **1992**, *114*, 1308−12.
(25) Ellis, P. E., Jr.; Lyons, J. E. *Coord. Chem. Rev.* **1990**, *105*, 181−93.
(26) Ellis, P. E., Jr.; Lyons, J. E. *Prepr.—Am. Chem. Soc., Div. Pet. Chem.* **1990**, *35*, 174−8.
(27) Moore, K. T.; Horvath, I. T.; Therien, M. J. *Inorg. Chem.* **2000**, *39*, 3125−3139.
(28) Moore, K. T.; Fletcher, J. T.; Therien, M. J. *J. Am. Chem. Soc.* **1999**, *121*, 5196−5209.
(29) Goll, J. G.; Moore, K. T.; Ghosh, A.; Therien, M. J. *J. Am. Chem. Soc.* **1996**, *118*, 8344−8354.
(30) DiMagno, S. G.; Wertsching, A. K.; Ross, C. R., II. *J. Am. Chem. Soc.* **1995**, *117*, 8279−80.
(31) DiMagno, S. G.; Williams, R. A.; Therien, M. J. *J. Org. Chem.* **1994**, *59*, 6943−8.
(32) Leroy, J.; Bondon, A.; Toupet, L.; Rolando, C. *Chem.—Eur. J.* **1997**, *3*, 1890−1893.
(33) Porhiel, E.; Bondon, A.; Leroy, J. *Tetrahedron Lett.* **1998**, *39*, 4829−4830.
(34) Porhiel, E.; Bondon, A.; Leroy, J. *Eur. J. Inorg. Chem.* **2000**, 1097−1105.
(35) Smirnov, V. V.; Woller, E. K.; Tatman, D.; DiMagno, S. G. *Inorg. Chem.* **2001**, *40*, 2614−2619.
(36) Nelson, A. P.; DiMagno, S. G. *J. Am. Chem. Soc.* **2000**, *122*, 8569−8570.
(37) Smirnov, V. V.; Woller, E. K.; DiMagno, S. G. *Inorg. Chem.* **1998**, *37*, 4971−4978.
(38) Woller, E. K.; DiMagno, S. G. *J. Org. Chem.* **1997**, *62*, 1588−1593.
(39) D'Souza, F.; Villard, A.; Van Caemelbecke, E.; Franzen, M.; Boschi, T.; Tagliatesta, P.; Kadish, K. M. *Inorg. Chem.* **1993**, *32*, 4042−8.
(40) Sun, H.-R.; Zhang, S.-Y.; Xu, J.-Q.; Yang, G.-Y.; Shi, T.-S. *J. Electroanal. Chem.* **1998**, *455*, 57−68.

Table 1. Redox Potential Data and Heterogeneous ET Kinetic Rate Constants for $CoF_{28}TPP$, $CoF_{20}TPP$, CoF_8TPP, and CoTPP in Benzonitrile Containing 0.1 M $TBAPF_6$ (E/V vs Ag/Ag^+)

	oxidation					reduction		
compd	third	second	$^a\Delta E_{2-1}{}^O$	first	$^b\Delta E_{O-R}$	first	$^c\Delta E_{2-1}{}^R$	second
CoTPP	1.151 (3.5×10^{-3})[d]	0.875 (3.6×10^{-3})	0.722	0.153 (1.8×10^{-3})	1.327	−1.174 (4.1×10^{-3})	1.111	−2.285
CoF_8TPP	1.368 (3.0×10^{-3})	1.210 (3.0×10^{-3})	0.877	0.333 (2.7×10^{-5})	1.187	−0.854 (3.8×10^{-3})	1.038	−1.892 (4.2×10^{-3})
$CoF_{20}TPP$	1.515	1.287	0.980	0.307 (5.9×10^{-6})	1.242	−0.935 (5.2×10^{-3})	1.000	−1.935
$CoF_{28}TPP$		1.675	1.119	0.556 (1.3×10^{-7})	1.140	−0.584 (2.7×10^{-3})	0.903	−1.487 (3.8×10^{-3})
ZnTPP[e]		1.16	0.36	0.80	2.13 (586)[f]	−1.33	0.33	−1.66
ZnF_8TPP[e]		1.36	0.10	1.26	2.29 (573)[f]	−1.03		
$ZnF_{28}TPP$[e]				1.70	2.33 (568)[f]	−0.63	0.41	−1.04

[a] $\Delta E_{2-1}{}^O$ is the potential separation between the first and the second oxidation. [b] ΔE_{O-R} is the potential separation between the first reduction and the first oxidation. [c] $\Delta E_{2-1}{}^R$ is the potential separation between the first and the second reduction. [d] The data in the parentheses are the heterogeneous ET kinetic rate constants in units of $cm \cdot s^{-1}$. [e] Data are from ref 38 in methylene chloride containing 0.1 M $TBAPF_6$, vs Ag/AgCl. Fc/Fc^+ was incorporated as an internal standard ($E_{1/2} = 0.48$ V vs Ag/AgCl). [f] Data in parentheses indicate the position of the Q(0,0) transition of neutral compound in methylene chloride (in nm).

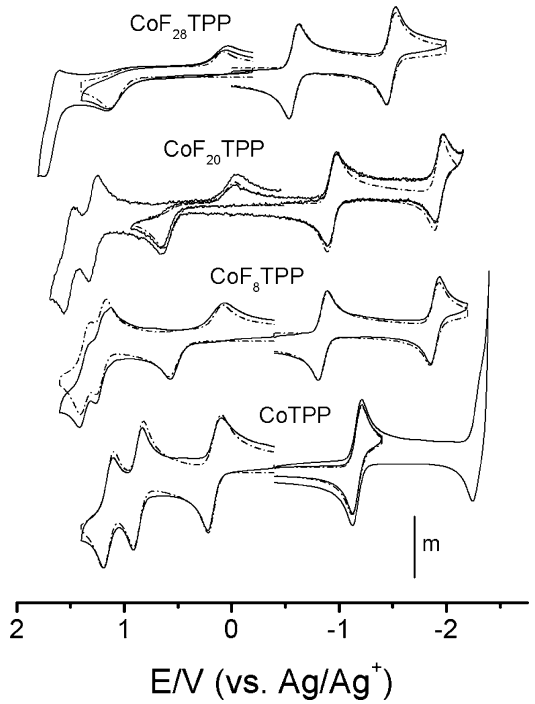

Figure 1. Cyclic voltammograms and digital simulation results of $CoF_{28}TPP$, $CoF_{20}TPP$, CoF_8TPP, and CoTPP in benzonitrile containing 0.1 M $TBAPF_6$ as supporting electrolyte. Scan rate = 100 mV/s. The solid lines are the experimental results; the broken lines are the digital simulation results. The scaling factor $m = 5$ μA for $CoF_{28}TPP$, CoF_8TPP, and CoTPP, and $m = 2.5$ μA for $CoF_{20}TPP$.

reactions, digital simulation, near-IR spectroscopy, FTIR spectroelectrochemistry, and semiempirical calculations are provided in the Supporting Information.

Results and Discussion

Cyclic Voltammetry. Cyclic voltammograms along with the corresponding simulation of the current/potential response for $CoF_{28}TPP$, $CoF_{20}TPP$, CoF_8TPP, and CoTPP in benzonitrile containing 0.1 M $TBAPF_6$ as supporting electrolyte are shown in Figure 1; the potentiometric data are summarized in Table 1. The four cobalt porphyrins undergo two quasireversible one electron reduction processes in benzonitrile; the first electron reduces the metal center ($Co^{2+/1+}$), while the second reduces the porphyrin ring π-system to form the corresponding radical dianion. The identities of the species generated by the sequential reduction processes were confirmed by in situ spectroelectrochemical studies (vide infra). Either two (for $CoF_{28}TPP$) or three (for $CoF_{20}TPP$, CoF_8TPP, and CoTPP) oxidation processes were observed within the available benzonitrile potential window.

As expected, fluorine substitution induces positive shifts ($\Delta E = E^\circ_{CoFnTPP} - E^\circ_{CoTPP}$) in the formal potentials relative to CoTPP. The largest potential shifts are $\Delta E^{(-1/-2)} = 798$ mV and $\Delta E^{(+1/+2)} = 800$ mV for the first porphyrin ring reduction and the first porphyrin ring oxidation waves of $CoF_{28}TPP$. In contrast, other halogenated metalloporphyrins, such as $ZnCl_8TPP$, $ZnCl_{28}TPP$, $ZnBr_8TPP$, and $CoBr_8TPP$, typically show larger potential shifts for ring reduction processes than for ring oxidation, an observation generally attributed to the nonplanar conformations observed in porphyrins substituted with the heavier halogens.[41,42] These effects are not observed with $CoF_{28}TPP$, which was shown to have a planar core conformation in both its high-spin and low-spin states.[37]

The formal potentials associated with metal-centered oxidation and reduction reactions of $CoF_{28}TPP$ and CoF_8TPP are shifted less than those of the corresponding porphyrin-centered redox events, due to the attenuation of the substituent effect by the macrocycle framework (Table 1). The differential shifts in the ring and metal electrochemical potentials are also evident in the energies of the ligand to metal charge transfer bands on the red edge of the electronic spectrum; these bands move to higher energy with increasing fluorine substitution (see Supporting Information).

(41) Bhyrappa, P.; Krishnan, V. *Inorg. Chem.* **1991**, *30*, 239−45.
(42) Ochsenbein, P.; Ayougou, K.; Mandon, D.; Fischer, J.; Weiss, R.; Austin, R. N.; Jayaraj, K.; Gold, A.; Terner, J.; Fajer, J. *Angew. Chem.* **1994**, *106*, 355−7. (See also: *Angew. Chem., Int. Ed. Engl.* **1994**, *106* (3), 348−50.)

Heterogeneous Electron Transfer Rate Constants. The shapes of the first oxidation waves ($Co^{2+/3+}$) in cyclic voltammograms of CoTPP, CoF_8TPP, $CoF_{20}TPP$, and CoF_{28}-TPP are strikingly different (Figure 1); the potential separation of the $Co^{2+/3+}$ anodic and cathodic peaks is 0.13 V for CoTPP, 0.50 V for CoF_8TPP, and 1.10 V for $CoF_{28}TPP$ at a sweep rate of 0.1 V/s. These data indicate that the $Co^{2+/3+}$ heterogeneous ET kinetic rate constant (k_{el}) is reduced in the fluorinated porphyrins. In contrast, other halogenated cobalt porphyrins, such as $CoBr_xTPP$, show enhanced ET rates: peak-to-peak separations for the $Co^{2+/3+}$ process decrease with increasing β-Br substitution.[43]

The results of cyclic voltammetric digital simulations are indicated as broken lines in Figure 1. (Details are given in the Supporting Information.) The simulation data show that k_{el} for the $Co^{2+/3+}$ process varies by more than 4 orders of magnitude for the cobalt porphyrins studied here (Table 1). Only the $Co^{2+/3+}$ reactions exhibit a large difference in the heterogeneous ET kinetic rate constants; k_{el} does not vary by more than a factor of 3 for the other electrode reactions. To exclude a substituent-induced change in the electron transfer site (metal- vs ring-localized ET) as an explanation for the varied heterogeneous ET kinetics of these fluorinated porphyrins, we performed in situ spectroelectrochemistry, bulk electrolysis, and ^{19}F NMR experiments to characterize definitively the products of each electrochemical process shown in Figure 1.

UV−vis Spectroelectrochemistry. Figure 2 shows the changes in the UV−vis spectra of $CoF_{28}TPP$, CoF_8TPP, and CoTPP in benzonitrile containing 0.1 M $TBAPF_6$ for the four reported redox processes. No low energy transitions indicative of porphyrin ring radical species are evident after the first oxidation (Figure 2A) or the first reduction (Figure 2C), indicating that these redox events are primarily metal-centered.[44] Further oxidation (Figure 2B) or reduction (Figure 2D) leads to the telltale signature of ring-centered processes, broad absorbance bands in the red to near-IR region.[45] To support the assignments that the first oxidation and reduction processes are metal-centered for $CoF_{28}TPP$, electrolyte solutions (0.1 M $TBAPF_6$ in benzonitrile) of $[CoF_{28}TPP]^{-1}$ and $[CoF_{28}TPP]^{+1}$ were analyzed by ^{19}F NMR and found to be diamagnetic. The chemical shifts of the porphyrin ring fluorine signals are an important diagnostic for metal electron density; accordingly, the chemical shift values for the ions ($[CoF_{28}TPP]^{-1}$, $\delta = -152.7$ ppm; $[CoF_{28}TPP]^{+1}$, $\delta = -142.8$ ppm) bracketed the benchmark value for $ZnF_{28}TPP$ ($\delta = -145.4$ ppm).[35,38]

Homogeneous ET Self-Exchange Rates. Marcus's semiclassical description of outer sphere ET[46−52] and the Marcus

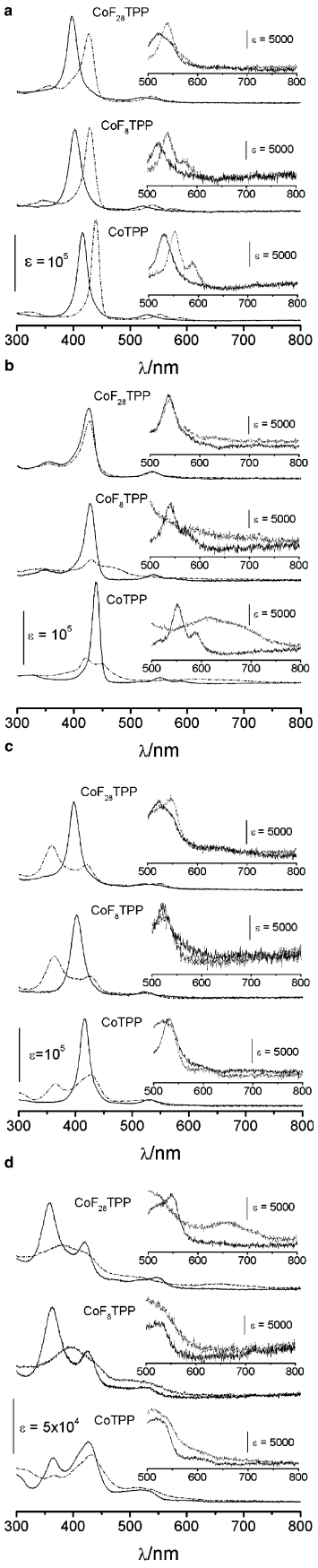

Figure 2. In situ UV−vis spectroelectrochemistry of $CoF_{28}TPP$, CoF_8-TPP, and CoTPP in benzonitrile, 0.1 M $TBAPF_6$: (A) first oxidation, (B) second oxidation, (C) first reduction, (D) second reduction.

(43) Kadish, K. M.; Li, J.; Van Caemelbecke, E.; Ou, Z.; Guo, N.; Autret, M.; D'Souza, F.; Tagliatesta, P. *Inorg. Chem.* **1997**, *36*, 6292−6298.
(44) Kadish, K. M.; Mu, X. H.; Lin, X. Q. *Inorg. Chem.* **1988**, *27*, 1489−92.
(45) Fajer, J.; Borg, D. C.; Forman, A.; Dolphin, D.; Felton, R. H. *J. Am. Chem. Soc.* **1970**, *92*, 3451−9.
(46) Marcus, R. A. *J. Chem. Phys.* **1965**, *43*, 679−701.
(47) Marcus, R. A. *J. Chem. Phys.* **1956**, *24*, 966−78.
(48) Marcus, R. A. *J. Chem. Phys.* **1957**, *26*, 872−7.
(49) Marcus, R. A. *J. Chem. Phys.* **1957**, *26*, 867−71.
(50) Marcus, R. A. *Discuss. Faraday Soc.* **1960**, 21−31.

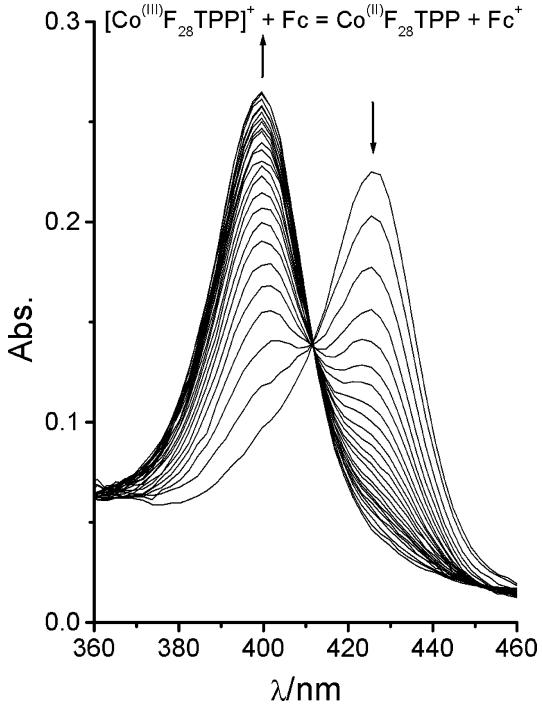

Figure 3. UV−vis spectral change during the ET reaction of $[CoF_{28}TPP]PF_6$ with excess ferrocene. Time: 0−1 s.

cross-reaction relationship[51] (eq 1) were used to estimate the self-exchange rate constants of $CoF_{28}TPP$, $CoF_{20}TPP$, CoF_8-TPP, and CoTPP (Table 3).

$$k_{12} = (k_{11}k_{22}K_{12}f_{12})^{1/2} \quad (1a)$$

$$\ln f_{12} = (\ln K_{12})^2/4 \ln(k_{11}k_{22}/Z_{11}Z_{22}) \quad (1b)$$

In eq 1, k_{12} is the cross-reaction rate constant, k_{11} and k_{22} are the self-exchange rate constants for the two redox partners, f_{12} is a correction factor (generally close to 1), K_{12} is the cross-reaction equilibrium constant, which is calculated from the difference in the redox potentials of the two species, and Z_{11} and Z_{22} are collision frequencies.

To determine k_{ex} for $CoF_{28}TPP$, the reductions of CoF_{28}-$TPP(PF_6)$ by ferrocene and dimethylferrocene were followed by stopped flow methods. Ferrocenes were selected as reducing agents because their k_{ex} values are well-established and have been shown to be relatively solvent insensitive.[53] The time-dependent decrease in Soret band intensity of rapidly mixed acetonitrile solutions (0.05 M $NaPF_6$ and 0.05 M $TBAPF_6$) containing $CoF_{28}TPP(PF_6)$ and ferrocene was followed by UV−vis spectroscopy (Figure 3). With excess ferrocene present (>20 times porphyrin concentration), good pseudo-first-order kinetic behavior was observed; the pseudo-first-order rate constants varied linearly with ferrocene concentration (see Supporting Information). At 25 °C, the cross-reaction rate constant was 6.4×10^4 M^{-1} s^{-1} (Table 2), yielding $k_{ex} = 7.0 \times 10^{-4}$ M^{-1} s^{-1} for $CoF_{28}TPP$. Similar studies with dimethylferrocene yielded $k_{ex} = 8.9 \times 10^{-4}$ M^{-1} s^{-1} for $CoF_{28}TPP$; thus, we assigned the average value (8×10^{-4} M^{-1} s^{-1}) as the standard for further studies.

Table 2. Summary of Cross-Reaction Data

reductant	oxidant	$-\Delta E^{o\prime}$ (V)	$-\Delta G$ (kcal/mol)	k_{ij} (M^{-1} s^{-1})
Fc[a]	$CoF_{28}TPP^+$	0.382	8.82	6.0×10^4
Me_2Fc[a]	$CoF_{28}TPP^+$	0.501	11.5	4.9×10^5
$CoF_{20}TPP$[b]	$CoF_{28}TPP^+$	0.249	5.64	16.3
$CoF_{20}TPP$[b]	CoF_8TPP^+	0.026	0.60	30.7
CoTPP[b]	$CoF_{28}TPP^+$	0.403	9.30	9.73×10^3

[a] These data result from stopped flow experiments conducted in CH_3CN (0.05 M $NaPF_6$, 0.05 M $TBAPF_6$). [b] These data were gathered by conventional, time-resolved UV−vis spectroscopy (benzonitrile, 0.1 M $TBAPF_6$).

Table 3. Self-Exchange Rate Constants of Cobalt Porphyrins and Benchmark Compounds

redox couple	k_{ex} (M^{-1} s^{-1})	ref
$CoF_{28}TPP^+/CoF_{28}TPP$	8.0×10^{-4} [a]	this work
$CoF_{20}TPP^+/CoF_{20}TPP$	20.4	this work
CoF_8TPP^+/CoF_8TPP	16.8	this work
$CoTPP^+/CoTPP$	1.8×10^4	this work
Fc^+/Fc	6.5×10^6	53
$CoTPP(Py)_2^+/CoTPP(Py)_2$	9.7	6
$Co(Phen)_3^{3+}/Co(Phen)_3^{2+}$	44	72
CoTTPCl/CoTTP[b]	2.7×10^4	73

[a] An average value (see text). [b] TTP is 5,10,15,20-tetratolylporphyrin.

Because the Soret band absorption energies differ significantly for the β-fluorinated and β-unsubstituted compounds, cross-reaction rates (Table 2) could be measured easily for the following pairs of cobalt porphyrins: $CoF_{28}TPP(PF_6)$ and $CoF_{20}TPP$, $CoF_8TPP(PF_6)$ and $CoF_{20}TPP$, and $CoF_{28}TPP$-(PF_6) and CoTPP. These reactions were sufficiently slow (Figure 4) to be followed by conventional UV−vis spectroscopy. Measured values for k_{ex} vary over a 10^7 range and mirror the results of the heterogeneous electron transfer experiments; the more fluorinated porphyrins exhibit reduced ET rates for the $Co^{2+/3+}$ process. Thus, specific electrode interactions are not the origin of the unusual electrochemical kinetic behavior of the fluorinated complexes, and unusually large reorganization energies (λ) are implicated as the likely source of the greater activation barrier for ET.

Structure of $Br[CoF_{28}TPP]\cdot CH_3CN$. We obtained single crystal X-ray diffraction data for $Br[CoF_{28}TPP]$ to identify a possible structural source for the substantial reorganization energies associated with the oxidation of $CoF_{28}TPP$. The structure of the acetonitrile complex, obtained by chemical oxidation of $CoF_{28}TPP$ with bromine, is rendered in Figure 5. $F_{28}TPP$ is somewhat unusual among the β-perhalogenated tetraarylporphyrins in that it supports a stable, planar conformation, as is shown by X-ray crystal structure determinations of the free base[54] and of its rhodium[36] and zinc[38] chelates. Two structures also indicate that $CoF_{28}TPP$ is planar.[37] In contrast, the acetonitrile complex of $Br[CoF_{28}$-$TPP]$ is significantly ruffled. The largest displacements from the mean plane of the ring (av = 0.48 Å) occur at the *meso* positions. In terms of its degree of nonplanarity, the structure

(51) Marcus, R. A. *J. Phys. Chem.* **1963**, *67*, 853−7.
(52) Marcus, R. A.; Eyring, H. *Annu. Rev. Phys. Chem.* **1964**, *15*, 155−96.
(53) Nelsen, S. F.; Ismagilov, R. F.; Gentile, K. E.; Nagy, M. A.; Tran, H. Q.; Qu, Q.; Halfen, D. T.; Odegard, A. L.; Pladziewicz, J. R. *J. Am. Chem. Soc.* **1998**, *120*, 8230−8240.
(54) Leroy, J.; Bondon, A.; Toupet, L. *Acta Crystallogr., Sect. C: Cryst. Struct. Commun.* **1999**, *C55*, 464−466.

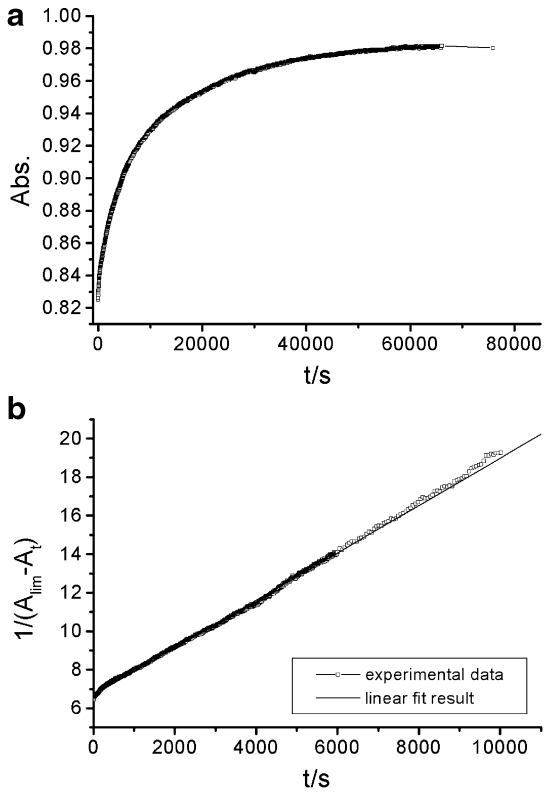

Figure 4. Top: Plot of the single wavelength (396 nm) absorbance change vs time for the cross-reaction of $[CoF_8TPP]^+$ and $CoF_{20}TPP$. Bottom: Plot of $1/(A_{lim} - A_t)$ vs time for the same data.

of $Br[CoF_{28}TPP]\cdot CH_3CN$ falls within the range seen in the structures of Co^{3+} derivatives of TPP.[55−61] The porphyrin core structure (Co−N bonds lengths average 1.971(6) Å, Co is displaced 0.01 Å from the mean plane of the nitrogen atoms, Table 4) is also unremarkable. For similarly ruffled Co^{3+}TPP derivatives, the Co−N bond lengths average 1.955,[62] 1.964,[63] and 1.975 Å,[64] respectively, for the aquachloro, diaquaperchlorate, and chloropyridine complexes. Although no definitive conclusions about the solution structure (where PF_6 is the counterion and benzonitrile or CH_3CN is the coordinating solvent) can be based upon the solid state structure, the available data indicate that there is nothing manifestly unusual about the type or degree of nonplanarity or the metal nitrogen bonding in $Br[CoF_{28}TPP]\cdot CH_3CN$.

(55) Goodwin, J.; Bailey, R.; Pennington, W.; Rasberry, R.; Green, T.; Shasho, S.; Yongsavanh, M.; Echevarria, V.; Tiedeken, J.; Brown, C.; Fromm, G.; Lyerly, S.; Watson, N.; Long, A.; De Nitto, N. *Inorg. Chem.* **2001**, *40*, 4217−4225.
(56) Munro, O. Q.; Shabalala, S. C.; Brown, N. J. *Inorg. Chem.* **2001**, *40*, 3303−3317.
(57) Ohba, S.; Eishima, M.; Seki, H. *Acta Crystallogr., Sect. C: Cryst. Struct. Commun.* **2000**, *C56*, e555−e556.
(58) Tse, A. K. S.; Wang, R.-j.; Mak, T. C. W.; Chan, K. S. *Chem. Commun.* **1996**, 173−4.
(59) Bang, H.; Edwards, J. O.; Kim, J.; Lawler, R. G.; Reynolds, K.; Ryan, W. J.; Sweigart, D. A. *J. Am. Chem. Soc.* **1992**, *114*, 2843−52.
(60) Yamamoto, K.; Iitaka, Y. *Chem. Lett.* **1989**, 697−8.
(61) Doppelt, P.; Fischer, J.; Weiss, R. *J. Am. Chem. Soc.* **1984**, *106*, 5188−93.
(62) Iimura, Y.; Sakurai, T.; Yamamoto, K. *Bull. Chem. Soc. Jpn.* **1988**, *61*, 821−6.
(63) Masuda, H.; Taga, T.; Osaki, K.; Sugimoto, H.; Mori, M. *Bull. Chem. Soc. Jpn.* **1982**, *55*, 4−8.
(64) Sakurai, T.; Yamamoto, K.; Seino, N.; Katsuta, M. *Acta Crystallogr., Sect. B* **1975**, *B31*, 2514−17.

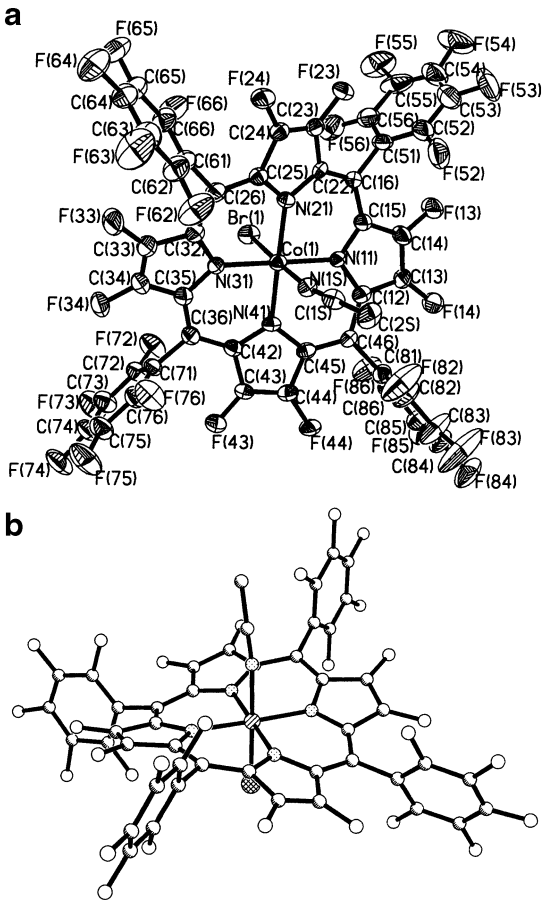

Figure 5. Perspective drawings from the X-ray crystal structure determination of $Br[CoF_{28}TPP]\cdot CH_3CN$. The top figure is drawn with 30% thermal ellipsoids.

Table 4. Summary of Structural Parameters for $Br[CoF_{28}TPP]\cdot CH_3CN$

Selected Bond Lengths and Angles

Co1−N21	1.965(5)	N21−Co1−N11	89.4(2)	C12−N11−C15	106.5(6)
Co1−N11	1.968(6)	N21−Co1−N31	90.6(2)	C12−N11−Co1	125.6(5)
Co1−N31	1.973(6)	N11−Co1−N31	179.7(3)	C15−N11−Co1	127.9(5)
Co1−N41	1.977(6)	N21−Co1−N41	178.5(3)	N11−C12−C46	127.0(7)
Co1−N1S	1.990(7)	N11−Co1−N41	90.1(2)	N11−C12−C13	123.7(7)
Co1−Br1	2.3499(13)	N31−Co1−N41	89.9(2)	C46−C12−C13	123.7(7)
N11−C12	1.363(9)	N21−Co1−N1S	89.0(3)	C14−C13−F14	126.6(8)
N11−C15	1.365(9)	N11−Co1−N1S	87.4(3)	C14−C13−C12	107.0(7)
C12−C46	1.396(10)	N31−Co1−N1S	92.9(3)	F14−C13−C12	126.2(7)
C12−C13	1.444(11)	N41−Co1−N1S	89.5(3)	C13−C14−F13	126.7(8)
C13−C14	1.322(11)	N21−Co1−Br1	90.77(18)	C13−C14−C15	107.7(7)
C13−F14	1.332(8)	N11−Co1−Br1	90.01(19)	F13−C14−C15	125.5(7)
C14−F13	1.350(9)	N31−Co1−Br1	89.7(2)	N11−C15−C16	124.5(7)
C14−C15	1.436(10)	N41−Co1−Br1	90.68(19)	N11−C15−C14	109.2(6)
C15−C16	1.388(10)	N1S−Co1−Br1	177.38(19)	C16−C15−C14	125.9(7)
C16−C22	1.379(10)	C1S−N1S−Co1	164.9(7)	C22−C16−C15	122.7(7)
C16−C51	1.501(10)			C22−C16−C51	118.3(7)
				C15−C16−C51	118.8(7)

Average Bond Lengths

Co−N	C_α−N	C_α−C_β	C_β−C_β	C_α−C_m	C_β−F_β
1.971	1.370	1.437	1.324	1.386	1.339

Thus, the solid state structure provides no obvious clue as to the source of the "extra" reorganization energy associated with the oxidation of $CoF_{28}TPP$ in comparison to CoTPP.

IR Spectroelectrochemistry. Difference IR spectroelectrochemical experiments were performed to interrogate axial ligation during the $Co^{2+/3+}$ oxidation. Prominent IR bands were observed at 2293.5 cm^{-1} ($CoF_{28}TPP$), 2292.5 cm^{-1}

(CoF_8TPP), and 2291.1 cm^{-1} (CoTPP) attributable to axial coordination of benzonitrile upon oxidation (see Supporting Information). These data are consistent with similar changes in benzonitrile coordination to Co^{3+} for each of the examples, suggesting that differences in axial ligation are not likely responsible for the larger reorganization energy observed for the fluorinated complexes; the changes in the benzonitrile stretching frequencies are markedly smaller than those associated with the porphyrin ring.

In addition to increasing the intensity of a number of absorption bands attributable to ring C−C and C−N stretching, fluorine substitution on the porphyrin ring gives rise to strong C−F IR signatures at 1699 cm^{-1} ($CoF_{28}TPP$) and 1688 cm^{-1} (CoF_8TPP). Upon either one-electron oxidation or reduction, these bands downshift dramatically (17 cm^{-1} for $CoF_{28}TPP$ and 15 cm^{-1} for CoF_8TPP). In contrast, when the metal charge is held constant and the ionic radius decreases, as in the series $ZnF_{28}TPP$, $CuF_{28}TPP$, $NiF_{28}TPP$, the porphyrin ring C−F stretching frequency increases. (C−F stretching frequencies of 1681, 1693, and 1695 cm^{-1} are observed for $ZnF_{28}TPP$, $CuF_{28}TPP$, and $NiF_{28}TPP$, respectively.)[65] Therefore, the increased charge on cobalt, rather than the conformational change due to the smaller ionic radius of Co^{3+}, is the most likely cause of downshifting upon oxidation. For fluorinated porphyrins, the bond weakening associated with repolarization is attributable to the substantial charge borne by the electronegative fluorine atoms in the Co^{2+} structure. In contrast, the IR frequency downshifts associated with $CoF_{28}TPP$ and CoF_8TPP reduction can be ascribed to population of a metal-centered orbital that leads to significant σ-antibonding interactions within the porphyrin ring.

Recent theoretical work (DFT B3LYP/6-31G(d)) comparing the vibrational spectra of octabrominated, octachlorinated, octafluorinated, and unsubstituted porphyrins indicates that ring fluorinated porphyrins show some marked differences compared to chlorinated or brominated counterparts.[66] The fluorinated porphyrins are unique in that high-frequency C−C and C−N in-plane bond vibrations are upshifted significantly relative to porphine.[66] Chlorinated and brominated porphyrins show substantial downshifts for these same modes. The trends described by DFT underlie a compact explanation for the slow kinetics associated with the $Co^{2+/3+}$ redox events; core size change requires significant reorganization in the porphyrin framework. Thus, the larger force constants for the bond vibrational modes of fluorinated porphyrins imply that the potential energy wells associated with expansion or dilation of the ring are steeper in the fluorinated compounds. This explanation is consistent with the IR-spectroelectrochemistry results and the X-ray crystallographic data.

PM3 Semiempirical Modeling of ET. To assess the impacts of halogenation and ion size upon inner sphere reorganization energies (λ_is) in metalloporphyrins, semiempirical calculations (PM3)[67,68] were performed on fluorinated and brominated model compounds. The model compounds were devoid of axial ligands, so that only those contributions to λ_i intrinsic to the porphyrin ligands were considered. Two simplifications were made in order to facilitate estimation of λ_i: (1) we chose Zn^{2+} as an example of a "large" +2 ion to obviate any complications arising from direct comparison of open-shell and closed-shell semiempirical calculations, and (2) the metal ions were constrained to the plane of the four nitrogen atoms in the porphyrin core for ruffled geometries to mimic the available structural data. Finally, we postulated that reorganization energies for the $Co^{2+/3+}$ self-exchange event are directly related to the inner sphere reorganization energies for the (computationally simpler) instantaneous (Zn^{2+}/Co^{3+}) metal ion exchange, with the understanding that the core size changes are somewhat larger for (Zn^{2+}/Co^{3+}) than they are for (Co^{2+}/Co^{3+}).[69] Consequently, λ_i is expected to be overestimated using this technique. Aside from the wrinkle of altering the identity of the ion, calculation of inner sphere reorganization energies by semiempirical methods has ample precedent.[70]

Optimized geometries for the Zn^{2+} and Co^{3+} derivatives of P, F_8P, Br_8P, F_8TPP, $F_{28}TPP$, and $Br_8F_{20}TPP$ were calculated. Conformational mapping was employed to find multiple local minima in several cases. Inner sphere reorganization energies derived from metal ion exchange were then calculated using the following equation:

$$\lambda_i = (E(CoL_{Zn}) - E(CoL_{Co})) + (E(ZnL_{Co}) - E(ZnL_{Zn}))$$

where $E(CoL_{Zn})$ is the calculated enthalpy of formation (ΔH_f) for the Co^{3+} porphyrin at the optimized Zn^{2+} porphyrin geometry, $E(CoL_{Co})$ is ΔH_f for the optimized Co^{3+} porphyrin, $E(ZnL_{Co})$ is ΔH_f for the Zn^{2+} porphyrin at the optimized Co^{3+} porphyrin geometry, and $E(ZnL_{Zn})$ is ΔH_f for the optimized Zn^{2+} porphyrin. Finally, energies of constrained ruffled geometries (transannular dihedral angles, e.g., C1−N21−N23−C14, were constrained to 50°, as described previously)[30,71] were calculated for all of the zinc complexes in order to give an estimate of the energy required for ruffling of the various porphyrins in the absence of metal ion exchange. The results of these calculations are summarized in Table 5. Initially, only the data from calculations involving a ruffled Co^{3+} porphyrin geometry are discussed (column 3 in Table 5).

ET in Ruffled Co^{3+} Porphyrins. Several interesting trends are seen in the data in Table 5. First, it is apparent that the calculations follow the general ordering seen in the

(65) Walters, V. A.; DiMagno, S. G.; Smirnov, V. V.; de Paula, J. C. *Book of Abstracts*, 215th National Meeting of the American Chemical Society, Dallas, TX, Mar 29−Apr 2, 1998; American Chemical Society: Washington, DC, 1998, INOR-320.
(66) Nguyen, K. A.; Day, P. N.; Pachter, R. *J. Chem. Phys.* **1999**, *110*, 9135−9144.
(67) Stewart, J. J. P. *J. Comput. Chem.* **1989**, *10*, 221−64.
(68) Stewart, J. J. P. *J. Comput. Chem.* **1989**, *10*, 209−20.
(69) Scheidt, W. R.; Lee, Y. J. *Struct. Bonding (Berlin)* **1987**, *64*, 1−70.
(70) Nelsen, S. F.; Blackstock, S. C.; Kim, Y. *J. Am. Chem. Soc.* **1987**, *109*, 677−82.
(71) Wertsching, A. K.; Koch, A. S.; DiMagno, S. G. *J. Am. Chem. Soc.* **2001**, *123*, 3932−3939.
(72) Haim, A.; Sutin, N. *Inorg. Chem.* **1976**, *15*, 476−8.
(73) Chapman, R. D.; Fleischer, E. B. *J. Am. Chem. Soc.* **1982**, *104*, 1582−7.

Table 5. Summary of Semiempirical (PM3) Calculations for Assorted Porphyrins[a]

compd	λ_{exp}[b]	λ_{ruf}[c]	λ_{sad}[d]	ΔH_{ruf}[e]	$\Delta\lambda$ (F_8)[f]	$\Delta\lambda$ (Br_8)[g]	$\Delta\lambda$ (Ph_4)[h]	$\Delta\lambda$ (C_6F_5)[i]
P		88.52		21.47	7.72	0.88	−9.76	
F_8P		96.24		20.25			−8.61	
Br_8P		89.39		20.32			−16.33	
TPP	36.17	78.75	71.46	18.87	8.88	−5.69		6.20
F_8TPP	52.89	87.63	69.49	12.15				9.29
Br_8TPP		73.06	59.79	12.35				0.65
F_{20}TPP	52.36	84.95	80.10	19.36	11.97	−11.23		
F_{28}TPP	76.11	96.92	85.12	11.19				
Br_8F_{20}TPP		73.72	63.03	10.58				

[a] All energies are reported in kcal/mol. [b] Calculated from the self-exchange ET rate constant and the Marcus equation. [c] Inner sphere reorganization energies for instantaneous metal ion exchange, calculated as described in the text. These data are obtained for ruffled Co(III) porphyrins. [d] Inner sphere reorganization energies for instantaneous metal ion exchange for saddled Co(III) porphyrins. [e] Energy calculated to distort Zn(II) porphyrin from its global minimum conformation to one in which the transannular dihedral angles, e.g., C1−N21−N23−C14, were constrained to 50°. [f] Difference in reorganization energy brought about by fluorination of the porphyrin ring for each of the porphyrins listed. [g] Difference in reorganization energy brought about by bromination of the porphyrin ring. [h] Difference in reorganization energy brought about by *meso*-phenyl substitution. [i] Difference in reorganization energy brought about by fluorination of the phenyl rings.

experimental results; compounds that exhibit small k_{ex} values are calculated to possess larger λ_i values. On the whole, the semiempirical model studies reasonably reproduce the experimental λ_i values, although the calculated values for λ_i are too large, as might be expected from the nature of the calculation, and do not show as much spread ($\lambda_i(F_{28}TPP) - \lambda_i(TPP) = 18$ kcal/mol) as the overall reorganization energies derived from the k_{ex} values ($\lambda_{(total)}(F_{28}TPP) - \lambda_{(total)}(TPP) = 30$ kcal/mol).

The second important trend evident in Table 5 is that reorganization energies are predicted to be strongly dependent upon β-substitution in sterically unencumbered porphyrins. In the series P, F_8P, and Br_8P, similar degrees of ruffling are observed for all three of the Co^{3+} porphyrins, but the calculated reorganization energies differ by a large margin. The larger reorganization energy calculated for F_8P indicates that fluorination (unlike bromination) significantly increases the energetic costs of porphyrin core expansion and contraction, consistent with DFT studies indicating that β-fluorination increases C−C and C−N stretching frequencies. Moreover, data from calculations of the constrained, ruffled Zn^{2+} complexes (Table 5, column 5) show that ruffling of the halogenated derivatives is somewhat easier than ruffling of ZnP, indicating that differences arising from nonplanarity cannot make a large contribution to the overall reorganization energy. These data and conclusions are consistent with complementary DFT results showing exceptionally low bending frequencies for ruffling of porphyrins generally, and for halogenated porphyrins in particular.[66]

Further substitution of the porphyrin macrocycle leads to more complex behavior. β-Halogenation of various porphyrins with relatively small fluorine atoms leads to uniformly larger λ_i values for all compounds studied (Table 5, column 6). In contrast, bromination of P results in a minimal change in λ_i, but a substantial lowering of λ_i is predicted for Br_8-TPP and Br_8F_{20}TPP (Table 5, column 7). For the latter compounds, steric clashes at the porphyrin periphery hinder contraction about the small Co^{3+} ion, resulting in reduced reorganization energies for the instantaneous exchange to the larger zinc ion.

The impact of *meso* phenyl substitution upon λ_i is indicated in column 8 of Table 5. Reorganization energies for the pairs P and TPP, F_8P and F_8TPP, and Br_8P and Br_8TPP were compared. In each case, addition of four *meso*-phenyl substituents leads to a decrease in the overall reorganization energy. By far the largest decrease in λ_i is seen for phenyl substitution of Br_8P; again, these calculations strongly suggest that steric effects limiting the extent of macrocycle contraction about the small Co^{3+} ion are responsible for the reduced λ_i values. The semiempirical calculations also predict that fluorination of the *meso*-phenyl substituents leads to high inner sphere reorganization energies, as is shown by examining the results from the pairs TPP and F_{20}TPP, F_8TPP and F_{28}TPP, and Br_8TPP and Br_8F_{20}TPP. These data are summarized in the last column of Table 5.

ET in Saddled Co^{3+} Porphyrins. Although oxidized cobalt porphyrins generally adopt ruffled conformations, very sterically demanding substituents allow access to low energy saddled conformations. Therefore, we explored how a change in ring conformation for the Co^{3+} state would alter λ_i. Local minima were found for saddled conformations of all of the Co^{3+} tetraarylporphyrins, and λ_i values were calculated as already described. Interestingly, the reorganization energies are predicted to be uniformly lower for this distortion mode (Table 5). Examination of the details used in the λ_i calculation indicate that the reduction in reorganization energy is due to the lower energy of the $E(ZnL_{Co})$ term for the saddled conformation compared to the ruffled geometry. In other words, the saddled core is more receptive to an instantaneous expansion in ion size than is a ruffled core. This result is easily interpreted: the saddled core structure reduces the σ-bonding overlap of the nitrogen orbitals with the metal (d_{z^2} and $d_{x^2-y^2}$) orbitals; thus, there is less energetic cost associated with changes in these orbitals' populations. Thus, substituents that induce a saddled conformation in the porphyrin ring should result in more rapid cobalt-centered ET reactions than are expected solely on the basis of electronic substituent effects. As the data in Table 5 show, the effect of varying the porphyrin distortion mode can be substantial.

Conclusions

These studies demonstrate that, under identical experimental conditions, ET self-exchange rate constants (k_{ex}) for the metal-centered oxidation in a series of closely related cobalt porphyrins can be modulated over 7 orders of magnitude by sterically undemanding substituent modification. Widely varying inner sphere reorganization energies for these closely related compounds are responsible for the differing ET rates. Spectroscopic, structural, and semiempirical (PM3) studies indicate that the divergent kinetic behavior of CoTPP, CoF_8TPP, CoF_{20}TPP, and CoF_{28}TPP first oxidations arises mainly from reorganization associated with porphyrin core dilation and contraction. Semiempirical theory

also shows that enforced saddling of the porphyrin ring dramatically reduces λ_i by minimizing M−N σ-bonding interactions.

The main conclusion from these studies, that the key features controlling electron transfer rate in cobalt porphyrins are (1) the degree of overlap between redox active metal orbitals and the porphyrin orbitals, and (2) substituents that alter the bond frequencies associated with porphyrin contraction and dilation, provide rational design principles for modulating ET rate constants in metalloporphyrins. These concepts also provide a plausible functional role for the ruffling often observed in the hemes of ET proteins such as cytochrome *c*. Such ruffling decreases porphyrin π−metal dπ interactions and minimizes porphyrin core contraction and expansion associated with the redox event, thereby providing small inner sphere reorganization energies and enhancing electron transfer rates in the natural systems. Confirmation of this proposed structure/function relationship could, in principle, be obtained by measuring ET rates in cytochrome *c* mutants in which the heme conformation is constrained to be saddled.

Acknowledgment. We thank the National Science Foundation (CHE-9817247) and the Office of Naval Research (N00014-00-1-0283) for support of this research.

Supporting Information Available: Details regarding (1) determination of formal redox potentials, (2) parameters for cyclic voltammetric digital simulation, (3) near-IR spectra for cobalt porphyrins and FTIR spectroelectrochemistry procedures and spectra, (4) procedures and data used to estimate ET self-exchange rate constants, (5) semiempirical calculations, and (6) the crystal structure refinement for $Br[CoF_{28}TPP]\cdot CH_3CN$. This material is available free of charge via the Internet at http://pubs.acs.org.

IC034705O